Pramana – J. Phys. (2016) 87: 7
DOI 10.1007/s12043-016-1218-6

Lifetime measurements in the yrast band of the gamma-soft nuclei ^{131}Ce and ^{133}Pr

R P SINGH[1,*], P JOSHI[2], S K CHAMOLI[3], S MURALITHAR[1], G MUKHERJEE[4], R K BHOWMIK[5] and S C PANCHOLI[3]

[1]Inter University Accelerator Centre (IUAC), P.O. Box 10502, New Delhi 110 067, India
[2]Department of Physics, University of York, Heslington, York Y0105DD, United Kingdom
[3]Department of Physics and Astrophysics, University of Delhi, Delhi 110 007, India
[4]Variable Energy Cyclotron Centre, 1/AF Bidhan Nagar, Kolkata 700 064, India
[5]IIEST, West Bengal, India
*Corresponding author. E-mail: rps_inuk@yahoo.com

MS received 20 March 2015; revised 6 July 2015; accepted 7 September 2015; published online 15 June 2016

Abstract. Lifetimes of excited states in the yrast band of the gamma-soft nuclei ^{131}Ce and ^{133}Pr have been measured using the recoil distance Doppler shift and Doppler shift attenuation methods. The yrast bands in ^{131}Ce and ^{133}Pr are based on odd decoupled neutron $\nu h_{11/2}$ high Ω and proton $\pi h_{11/2}$ low Ω orbitals, respectively. The triaxiality parameter extracted from the experimentally deduced values of transition quadrupole moments, within the framework of cranked Hartree–Fock–Bogoliubov (CHFB) and total Routhian surface (TRS) calculatons, is $\gamma \sim -80°$ for the band in ^{131}Ce at high spins, while for the band in ^{133}Pr, the value of γ is close to 0°. This agrees well with the γ shape polarization property of high and low $\Omega h_{11/2}$ orbitals in these gamma-soft nuclei.

Keywords. Lifetime measurements; RDM; Doppler-shifted attenuation method; total Routhian surface; triaxial-shape polarization.

PACS Nos 21.10.Tg; 23.20.−g; 21.10.Re; 27.60.+j

1. Introduction

Shape deformations in nuclei are related to the general phenomenon of spontaneous symmetry breaking in subatomic and mesoscopic sytems (first proposed by Jahn and Teller for molecules [1]). In nuclei, these occur due to the coupling between collective excitations of the nucleus and single-particle motion of the nucleons. As a result, prolate, oblate, octupole and even triaxial shapes are observed in nuclei, while the quest is on to look for even more exotic shapes such as tetrahedral or triangular shapes [2,3]. To understand microscopically the origin of these shape deformations, it is important to study the underlying nuclear level structure and the properties of various orbitals in which the nucleons move.

Nuclei in the light rare-earth region ($A \sim$130) exhibit a variety of rotational sequences that are associated with prolate, oblate, highly deformed prolate and triaxial shapes [4,5]. In particular, some of these nuclei are shown to possess shallow potential energy surfaces with respect to the triaxiality parameter γ (defined in the polar description of rotating quadrupole shapes [6]) and are thus ideal to study the γ-shape polarizing property of specific single-particle orbitals. The study by Paul *et al* [7] gave the first experimental evidence for the existence of collective oblate ($\gamma = -60°$ following the Lund convention [8]) and prolate bands ($\gamma = 0°$) in the ^{131}La nucleus. They linked these different shapes to high Ω (projection quantum number of single-particle angular momentum along the symmetry axis) $h_{11/2}$ neutron orbitals and low $\Omega h_{11/2}$ proton orbitals, respectively. However, only a few studies [5,9,10] have been reported focussing on the role of single-particle orbitals on shape parameters, extracted directly from lifetime measurements of the states.

The purpose of the present study is to examine the triaxial shape polarization property of high Ω neutron and low Ω proton $h_{11/2}$ orbitals through lifetime measurements. For this purpose, two odd-A nuclei, one

with an odd neutron (^{131}Ce) and another with an odd proton (^{133}Pr) were chosen. Earlier study of ^{131}Ce nucleus was done by Palacz *et al* [11] and of ^{133}Pr by Hildingsson *et al* [12] and Paul *et al* [10]. In ^{131}Ce, the yrast band is based on the decoupled odd neutron in high $\Omega h_{11/2}$ orbital, while in ^{133}Pr, the yrast band is based on the decoupled odd proton in low $\Omega h_{11/2}$ orbital. From earlier studies, both these nuclei have been inferred to possess quadrupole deformation β_2 of about 0.2 at low spin values in the yrast band. In the present study, lifetimes were measured using the plunger and Doppler-shifted attenuation (DSA) methods. Section 2 describes the details of the experiment for ^{131}Ce and in §3, the experimental results for ^{131}Ce are given. In §4 and §5, the details of the experiment for ^{133}Pr are presented. In §6, the experimental results are compared with the total Routhian surface calculations within the framework of the self-consistent cranked Hartree–Fock–Bogoliubov shell model (CHFB) with Woods–Saxon potential [13–15]. The summary is presented in §7.

2. Lifetime measurements in ^{131}Ce

2.1 *Experimental details*

Two experiments were carried out for lifetime measurements of excited states in ^{131}Ce in the yrast band based on the $\nu h_{11/2}$ orbital. The first experiment was done to measure lifetimes of the low-energy states using the recoil distance Doppler shift or the plunger technique. In the second experiment Doppler-shifted attenuation method (DSAM) was used to measure the lifetimes of higher lying members of the band. The fusion evaporation reaction ^{119}Sn(^{16}O,4n)^{131}Ce was used to populate high spin states in ^{131}Ce. In the plunger experiment, the beam energy was 86 MeV. The beam was delivered by the 15UD Pelletron accelerator at IUAC, New Delhi [16]. The target used was about 100 μg/cm^2 evaporated on gold backing having a thickness of about 1.5 mg/cm^2. This arrangement helped in proper stretching of the target over the cone of the plunger. Further details of the plunger device and the stretching mechanism can be found in refs [17,18]. The stopper consisted of another gold foil of thickness of about 7 mg/cm^2 which was stretched on another cone. The thickness of the stopper foil was sufficient to stop the recoils but allowed the beam to pass through.

The target and stopper foils form two parallel plates of a capacitor. The capacitance of the target–stopper foil assembly is inversely proportional to the distance between the target and the stopper foils. The capacitance is measured using the pulse technique [19]. A plot of (capacitance)$^{-1}$ vs. distance between the foils, varied by precision micromotors, was made. By extrapolation, the intercept of the curve on the distance axis gives the minimum distance d_0 (or 'zero-distance' in terms of micromotor reading) between the target and the stopper foils. This minimum distance d_0 was added to the movement made by the micromotors to get the flight distance. The minimum distance between the target and the stopper was found to be 12 μm in the present experiment. The data for the plunger experiment were collected for 14 different target–stopper distances ranging from 12 μm to about 1000 μm. During the experiment, a check on the capacitance variation was maintained to monitor the target–stopper distance due to the beam falling on the target and it was found to be less than ± 1 μm.

In the DSAM experiment, the target used was a self-supporting ^{119}Sn foil having a thickness of about 20 mg/cm^2 and the energy of the beam was 90 MeV. The thickness of the target which actually contributed to the production cross-section was estimated to be about 8 mg/cm^2. In both experiments, the ^{119}Sn target enrichment was about 93%. The emitted γ-rays in both plunger and DSAM experiments were detected using the gamma detector array (GDA) set-up at IUAC, consisting of 12 Compton-suppressed HPGe (CSGe) detectors and a 14-element BGO multiplicity filter. The HPGe detectors (each of about 23% efficiency) were placed at 50°, 98° and 144° with respect to the beam direction with four detectors at each angle. Further details of the GDA set-up can be seen in [18,20].

The data were collected with the hardware condition that two or more CSGe detectors fired in coincidence. Simultaneously, data from three CSGe detectors (each one at 50°, 98° and 144°) were also collected in singles mode with the multiplicity condition of at least one element of the BGO multiplicity detector fired in coincidence. The use of multiplicity condition reduced the low multiplicity gamma lines in the singles data. The relative efficiency and energy calibrations of the HPGe detectors were done using ^{133}Ba and ^{152}Eu radioactive sources.

2.2 *Data analysis of the plunger experiment*

The singles data were not used for lifetime analysis because of the strong interference of positron annhilation transition (511 keV) with the 510 keV ($15/2^- \rightarrow 11/2^-$) transition. The coincidence γ-ray data at different target–stopper distances were sorted into

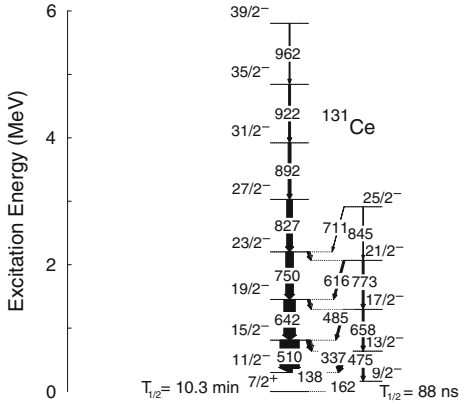

Figure 1. Partial level scheme of ^{131}Ce showing the yrast band based on decoupled neutron $h_{11/2}$ orbital (from refs [11,21]).

γ–γ matrices after gain matching different detectors to 0.5 keV per channel. Two types of γ–γ matrices were formed: (i) with all the detectors on one axis and the backward angle detectors on the other axis and (ii) with all the detectors on one axis and the forward angle detectors on the other axis. Partial level scheme of ^{131}Ce is shown in figure 1 depicting the yrast band based on the decoupled neutron $h_{11/2}$ orbital [11]. In figure 2, γ-ray spectra for four target–stopper distances at 144° with respect to the beam direction, generated with a gate on 162 keV transition ($9/2^- \rightarrow 7/2^+$) are shown. The $9/2^-$ state is an isomer with a half-life of 88 ns [21]. Gating on the 138 keV transition ($11/2^- \rightarrow 9/2^-$) was avoided due to the interference of the 137 keV transition arising from Coulomb excitation of the ^{181}Ta collimator inside the plunger device.

The coincidence time window, while sorting the γ–γ matrices, was kept 300 ns wide so that most of the decays from the $9/2^-$ state were accepted in the coincidence matrices. Shifted and unshifted peaks for the γ-rays of 510 keV ($15/2^- \rightarrow 11/2^-$) and 642 keV ($19/2^- \rightarrow 15/2^-$) can be clearly seen in figure 2. The 750 keV transition ($23/2^- \rightarrow 19/2^-$) (not shown in figure 2) was totally shifted at the minimum target–stopper distance and thus did not qualify for lifetime analysis with the plunger technique. We would like to mention that the statistics in coincidence data was not sufficient for the differential decay curve analysis which requires setting a gate on the shifted component of the transition directly feeding the level of interest [22].

The ratio of the intensity of unshifted component and the total intensity (sum of the shifted and unshifted intensities) of the γ-ray was multiplied with relative intensity of the transition in the band to obtain normalized relative intensity. The decay of cascading levels is described by Bateman equations. These equations are implemented in the program LIFETIME [23]. The normalized unshifted intensities at different target–stopper distances were fitted using this program. The fitted decay curves for the normalized unshifted intensity of 510 keV and 642 keV transitions are shown in figure 3. The program LIFETIME allows to include the effect of unknown side-feedings in addition to the known feeding levels. The quadrupole moments for the states above $23/2^-$ determined from the present DSAM experiment were used to constrain the fit of the decay curves. An additional cascade feeding to the $15/2^-$ level was considered in the present analysis to fit the data (based

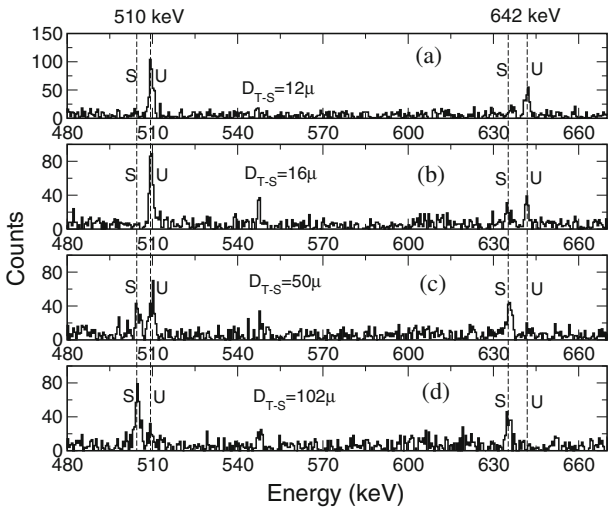

Figure 2. Shifted (S) and the unshifted (U) peaks for the 510 keV and 642 keV γ transitions in ^{131}Ce for different target-to-stopper distances (D_{T-S}) at 144° with respect to the beam direction with gate on 162 keV transition.

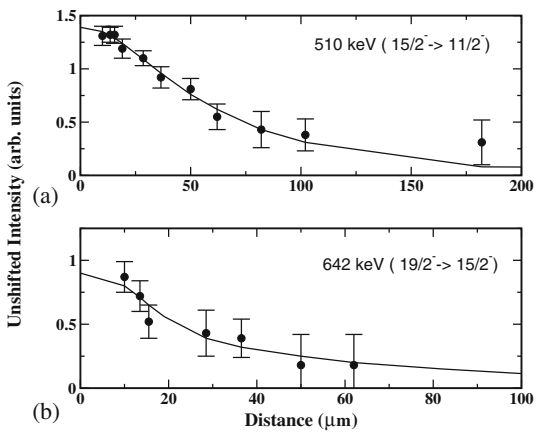

Figure 3. Decay curves of the normalized unshifted intensities for (**a**) 510 keV ($15/2^- \rightarrow 11/2^-$) and (**b**) 642 keV ($19/2^- \rightarrow 15/2^-$) transitions in the $\nu h_{11/2}$ yrast band of ^{131}Ce.

on the level scheme developed in [11]). Further, the progam LIFETIME also includes the effects of solid angle changes and deorientation during flight. The maximum error in the lifetime determination due to the deorientation effect was estimated to be about 3% in these measurements. The method adopted for this estimation is given in ref. [24]. The average velocity of recoils determined from the difference between the energy of the shifted and the unshifted peaks of gamma transitions was 1.20(4)% of the velocity of light. At this velocity, the change in solid angle due to the relativistic effect for inflight decays was estimated to be about 2.8%.

The errors were calculated by the least-square minimization package MINUIT [25] which includes the error routine MINOS in the program LIFETIME. The errors correspond to the change in the value of the parameter for a change of χ^2 value by one unit on both sides of the minimum.

2.3 *Data analysis of the DSAM experiment*

The γ-ray data from the DSAM experiment were sorted into two γ–γ matrices with a resolution of 0.5 keV per channel after gain matching of the HPGe detectors, for lifetime determination by the Doppler-broadened line shape (DBLS) analysis. One matrix consisted of all the dectectors on one axis and the backward (144°) ring detectors on the other axis, while the other matrix had all the detectors on one axis and the forward (50°) ring detectors on the other axis. The spectra from gates set on the 510, 642 and 750 keV transitions were summed up to improve the statistics for DBLS analysis. DBLS analysis was done using the program LINESHAPE [26]. The program uses Monte Carlo simulation technique to simulate the velocity histories of the recoiling nuclei. Five thousand recoil histories were generated at a time step of 0.002 ps. There are a number of prescriptions for the stopping power of recoils in the target and backing material. In this study, both the Ziegler's heavy-ion stopping power [27] and the shell-corrected Northcliffe and Schilling stopping powers [28] were used. The results were found to be in agreement within the error bars for both prescriptions and the results presented are an average of the two values, while the errors quoted are the larger error of the two values.

LINESHAPE program does a chi-square minimization of the fit for (i) the transition quadrupole moment Q_t for the level, (ii) the transition quadrupole moment for the modelled side-feeding Q_{SF}, (iii) the normalizing factor to normalize the intensity of the fitted transition at each angle, (iv) the intercept and the slope of the background, (v) mean lifetime τ_{SF} if a cascade side-feeding level is considered and (vi) the intensity of contaminant peaks. In the present analysis, four-level rotational band side-feeding and a cascade feeding for the level with $J^\pi = 27/2^-$ were considered for fitting the lineshapes. The value of the moment of inertia of the side-feeding band used was 30 $\text{MeV}^{-1}\hbar^2$ and this value was estimated from the yrast band. The intensities of feeding transitions were estimated based on the intensities of the cascading transitions in the band from the data at 98° and from the earlier study [29]. The average fitted value of the quadrupole moment for the side-feeding band was about 5 eb and long feeding times were not required to fit the lineshapes of the transitions in the yrast band. In figure 4, examples of the fitted Doppler-broadened lineshapes for backward and forward detectors for the 827 keV ($27/2^- \rightarrow 23/2^-$) and 922 keV ($35/2^- \rightarrow 31/2^-$) transitions in ^{131}Ce are shown. In the case of 922 keV γ-ray, the contaminant peaks at higher energies were not included in the fitting of lineshape at 144° because they do not interfere with it at this angle. The best fit was obtained by using the least square minimization procedures SEEK, SIMPLEX and MIGRAD outlined in ref. [26].

The 750 keV transition ($23/2^- \rightarrow 19/2^-$), which was observed to be totally shifted in the plunger experiment, did not show any significant angle-dependent lineshape. From the estimates of the stopping time of

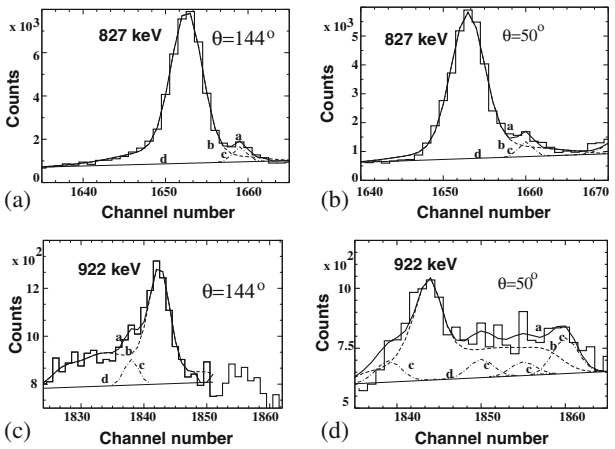

Figure 4. Doppler-broadened fitted line shapes (**a**) and (**b**) of 827 keV ($27/2^- \rightarrow 23/2^-$) and (**c**) and (**d**) of 922 keV ($35/2^- \rightarrow 31/2^-$) transitions in ^{131}Ce for backward (144°) and forward (50°) detectors respectively. In each frame, the curve a is the overall fit to the line shape, curve b is the line shape fit for the transition. The peaks labelled c are perturbing contributions from other γ-rays in the region of line shape of interest and d denotes the background line.

the recoils in the thick Sn target, a lower limit on the mean lifetime of the $23/2^-$ state was estimated to be 1.3 ps, while the upper limit estimated from the plunger experiment was about 3 ps. The error analysis for the fitted quantities was done using the package MINOS (which is also part of the program LINESHAPE), as described above for the plunger data analysis. The use of a thick target causes variation in the production cross-section as the beam energy decreases in the target up to the Coulomb barrier (about 70 MeV in the present case). We have estimated the error due to this variation to be a maximum of about 5%. The uncertainities in the stopping powers are about 5–10% and we have thus, fixed a minimum error of 10% on the extracted values of lifetimes.

The use of thick target is also expected to cause a broad entry point. However, a detailed study [30] (for a reaction very similar to the present reaction) showed that the uncertainties in the side-feeding pattern does not strongly affect (±15%) the extracted lifetimes and the uncertainties in side-feeding decrease with increasing spin. In view of the above observations, evaluation of the side-feeding by parameters $Q_{\rm SF}$, $\tau_{\rm SF}$ (explained above) through fitting the data in a wide range of values (for $Q_{\rm SF}$: 1–10 eb and for $\tau_{\rm SF}$: 0.05–3 ps) is a reasonable approximation. Further, as the estimated errors for the side-feeding parameters correspond to a confidence window of 68%, it includes uncertainties arising due to broad entry point to a large extent.

3. Experimental results for ^{131}Ce

The mean lifetimes (τ) and the transition quadrupole moments ($Q_{\rm t}$) extracted from the above analysis are tabulated in table 1 along with side-feeding lifetimes or quadrupole moments. Lifetime and transition quadrupole moment values for the states available from earlier measurements [31,32] are also given in table 1.

Transition quadrupole moments were determined from the extracted lifetimes of the states using the following rotor equation:

$$T(E2; I \to I-2) = 1.224.10^{12} E_\gamma^5 \langle I2K0|I-2K\rangle^2 \, Q_{\rm t}^2, \tag{1}$$

where γ-ray transition energy E_γ is in MeV, $Q_{\rm t}$ is in eb and transition probability T is in s^{-1}, the Clebsch–Gordan (CG) coefficient for non-axial shapes or mixed-K state in eq. (1) gets modified [33] to

$$\mathrm{CG} = \sum_K a_K(I) a_K(I-2) \langle I2K0|I-2K\rangle\,, \tag{2}$$

where $a_K(I)$ are the expansion coefficients of the state with angular momentum I in terms of states of pure K. For a rotation aligned state with a single quasiparticle of angular momentum j, $a_K(I)$ is given by [34]

$$a_K(I) = d^j_{jK}\left(\frac{\pi}{2}\right), \tag{3}$$

where $d^j_{\rm mm}(\beta)$ is a reduced rotation matrix element. However, in the present case, with $j = 11/2$, the difference in the value of CG coefficients calculated using

Table 1. Lifetime (τ) and transition quadrople moment ($Q_{\rm t}$) of the states in the yrast band based on neutron $h_{11/2}$ orbital in ^{131}Ce. The lifetime ($\tau_{\rm SF}$) or transition quadrople moment ($Q_{\rm SF}$) for the side-feeding levels used to fit the data along with values of lifetime from refs [31] and [32] with transition quadrupole moment extracted using eq. (1) are also tabulated for comparision.

		Present				Ref. [31]		Ref. [32]	
J_i^π	E_γ (keV)	τ (ps)	$Q_{\rm t}$ (eb)	$Q_{\rm SF}$ (eb)	$\tau_{\rm SF}$ (ps)	τ (ps)	$Q_{\rm t}$ (eb)	τ (ps)	$Q_{\rm t}$ (eb)
$15/2^-$	510	$9.6^{+1.9}_{-3.8}$	$2.93^{+0.6}_{-0.3}$	–	$1.0^{+0.1}_{-0.2}$	7.53(37)	3.24(8)	–	–
$19/2^-$	642	<7.31	>1.90	–	–	–	–	>4	<2.5
$23/2^-$	750	>1.3	<2.85	–	–	–	–	1.44(54)	2.72(51)
$27/2^-$	827	$1.25^{+0.41}_{-0.25}$	$2.26^{+0.37}_{-0.23}$	–	$0.73^{+0.15}_{-0.12}$	–	–	1.23(23)	2.28(21)
$31/2^-$	892	$0.51^{+0.05}_{-0.05}$	$2.66^{+0.13}_{-0.12}$	$5.79^{+0.24}_{-0.28}$	–	–	–	<1.04	>2.03
$35/2^-$	922	$0.60^{+0.11}_{-0.10}$	$2.43^{+0.22}_{-0.20}$	$5.01^{+1.44}_{-0.77}$	–	–	–	–	–
$39/2^-$	962	<0.54	>2.29	–	–	–	–	–	–

eq. (2) compared to $\langle I2K0|I-2K\rangle$ in eq. (1) for $K = 1/2$ is atmost only a few percent. As this is much less than the experimental errors, a simpler eq. (1) was used to calculate the values of Q_t with $K = 1/2$ in table 1.

The lifetime results from the present measurements agree well within the error bars with those known from earlier measurements [31,32]. The transtion quadrupole moment (Q_t) values are plotted as a function of initial spin in figure 5. It can be seen from the plot that the average value of the transition quadrupole moment is about 3 eb at the beginning of the band and then decreases to an average value of about 2.5 eb for spin beyond $12\hbar$.

4. Lifetime measurements in ^{133}Pr

4.1 *Experimental details*

The lifetimes of states in ^{133}Pr were measured by using the plunger technique. The high spin states in ^{133}Pr were populated using the reaction ^{118}Sn(^{19}F,4n)^{133}Pr at a beam energy of 92 MeV. The beam was delivered by the 15UD pelletron accelerator at IUAC, New Delhi. The ^{118}Sn target of $\sim$1 mg/cm^2 thickness (92% enriched) was rolled on a gold backing of about 3 mg/cm^2 thickness. The target was mounted such that the gold backing faced the beam. The beam energy was deliberately chosen slightly higher to compensate for the energy loss of the beam in the gold backing. The gold backing enabled proper stretching of the target. The stopper was also a gold foil of about 6 mg/cm^2 thickness. The same GDA set-up discussed above was used in this experiment. Gamma–gamma coincidence as well as multiplicity gated singles data were collected. However, the γ–γ coincidence data were not found suitable for analysis due to insufficient statistics. The multiplicity condition for the singles data required one or more BGO multplicity filter detectors to fire in coincidence with the Compton-suppressed HPGe detector. The distance calibration of the plunger device was done using the capacitance method (as described in §2.1) and the minimum target–stopper distance achieved during this experiment was about 7 μm. A variation of less than ± 1 μm was seen due to the beam impact on the target during experiment.

4.2 *Data analysis*

Three groups of spectra were formed with the data based on the detector angles, namely, 144° (backward angle), 98° (right angle) and 50° (forward angle). The multiplicity gated singles data from the detectors in each group were gain matched and added to give three sets of gain-matched data at the three angles. Figure 6 depicts the partial level scheme of ^{133}Pr based on refs [10,12]. In figure 7 shifted and unshifted γ-ray peaks for the 552, 709 and 682 keV transitions for four target–stopper distances are shown for the backward angle detectors. The normalized intensities of the shifted and unshifted components of γ transitions were extracted for different target–stopper distances. The normalization of data at different distances was done with the total intensity (sum of the shifted and unshifted intensities) of the transition. These intensities were then multiplied by the relative intensity (as observed in the present experiment) of the γ transition to get the normalized relative intensity; these intensities were then used for lifetime analysis using

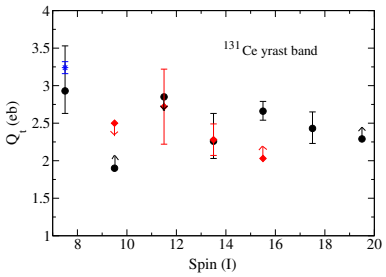

Figure 5. Experimentally determined transition quadrupole moment Q_t plotted against spin (I) $\hbar$ for the yrast states in ^{131}Ce based on $\nu h_{11/2}$ orbital. The values determined from the present study are denoted by circles, while those determined from lifetime values from refs [31] and [32] are denoted by star and diamond symbols respectively.

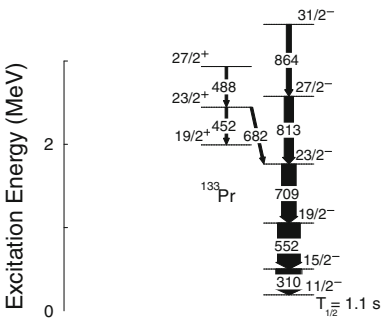

Figure 6. Partial level scheme of ^{133}Pr [10,12]. The yrast band based on $\pi h_{11/2}$ configuration is shown along with feeding to the $23/2^-$ state from a positive-parity band (the lower spin states below $19/2^+$ state are not shown). The width of the lines are approximately proportional to their intensities.

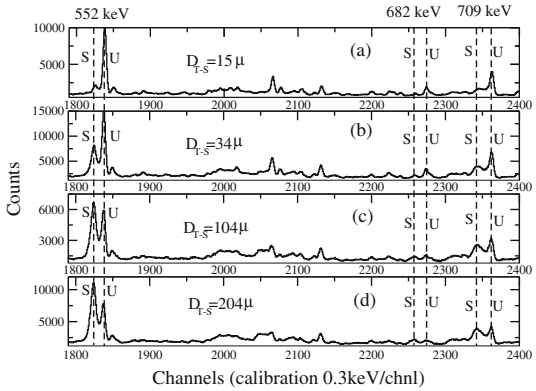

Figure 7. Unshifted and shifted peaks for 552 keV ($19/2^- \rightarrow 15/2^-$), 709 keV ($23/2^- \rightarrow 19/2^-$) and 682 keV ($23/2^+ \rightarrow 23/2^-$) transitions in ^{133}Pr. These spectra were generated from multiplicity-gated singles data with multiplicity gate >1; the HPGe detectors were at 144° with respect to beam direction.

the program 'LIFETIME' [23]. Representative fitted decay curves to these normalized relative intensties are shown in figure 8a–8c for the unshifted peaks of 310, 552 and 709 keV γ transitions of the yrast band (see figure 6).

In the program LIFETIME cascade side feeding as well as three-level band feeding from top of the band were modelled. Clues for modelling the feedings were taken from the level scheme of ^{133}Pr as established in [12]. The feeding time from the positive-parity band via the 682 keV transition ($23/2^+ \rightarrow 23/2^-$) was determined by extracting the lifetime of the $23/2^+$ state. This was done by fitting the normalized intensity of unshifted

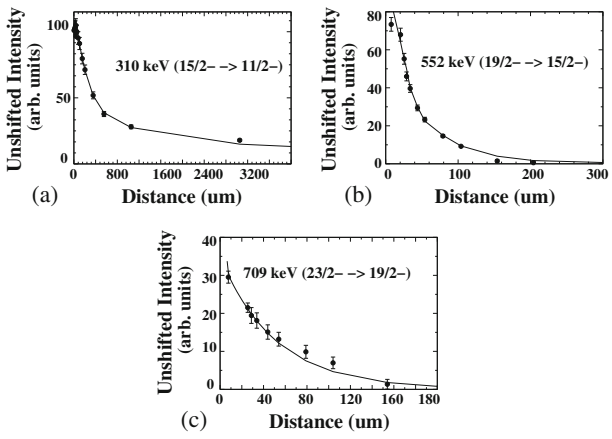

Figure 8. Fitted decay curves of the normalized intensities of unshifted peaks for (**a**) 310 keV ($15/2^- \rightarrow 11/2^-$), (**b**) 552 keV ($19/2^- \rightarrow 15/2^-$) and (**c**) 709 keV ($23/2^- \rightarrow 19/2^-$) transitions plotted as a function of target-to-stopper distance.

peak of 682 keV transition as a function of flight distance separately. The mean lifetime determined for the $23/2^+$ state was $14.0^{+2.7}_{-3.3}$ ps with a band feeding from $27/2^+$ state with an effective quadrupole moment of 3.3 eb. While fitting the intensities as a function of distance for the γ transitions of yrast states, this feeding time was used as a constraint (within the given errors), while the other feeding times were treated as free parameters.

The side-feeding intensities were estimated based on the present data and data from ref. [12]. A long feeding lifetime of about 1 ns for the cascade feeding the $15/2^-$ state had to be considered to get a good fit to the data. This was found to be reasonable due to a partial feeding to this level from a higher isomeric state at 2034 keV ($T_{1/2} \leq 35$ ns) [35] through the 1265 keV level (not shown in the partial level scheme in figure 6). The quadrupole moment for the modelled band feeding was restricted between 4 and 5 eb based on the quadrupole moment determined by Paul *et al* [10] for higher members of the band (at spins of about $20\hbar$). The errors were determined by the same procedure using the routine MINOS in the program LIFETIME and as discussed in §2.2.

5. Experimental results for ^{133}Pr

The mean lifetimes and the transition quadrupole moments extracted from the analysis are tabulated in table 2. For the yrast band based on decoupled $\pi h_{11/2}$ orbital we have assumed $K = 1/2$ in eq. (1) for the calculation of transition quadrupole moments. The lifetimes of $15/2^-$ and $19/2^-$ states determined by Klemme *et al* [31] are also tabulated along with the resultant transition quadrupole moments. Our results are in good agreement with these measurements. For the $23/2^+$ state the value of mean lifetime was determined by using a branching fraction of 0.71(8) for the 682 keV ($23/2^+ \rightarrow 23/2^-$) transition.

Figure 9 shows a plot of the transition quadrupole moments as a function of the initial spin for members of the yrast band. It can be seen from this plot that at the beginning of the band, the transition quadrupole moment is about 3.6 eb which shows marginal decrease (if at all) at higher spins.

6. Shape calculations and discussion

6.1 ^{131}*Ce nucleus*

Total Routhian surface (TRS) calculations [13–15] based on cranked Hartree–Fock–Bogoliubov and Strutinsky

Table 2. Mean lifetimes (τ) and transition quadrupole moment (Q_t) determined for the states in ^{133}Pr along with the energies of the γ-rays (E_γ) and spin, parity of the de-exciting level (J^π). Values of mean lifetime of side-feeding levels (τ_{SF}), lifetimes from ref. [31] and the extracted transition quadrupole moment using eq. (1) are also tabulated.

		Present			Ref. [31]	
J_i^π	E_γ (keV)	τ (ps)	Q_t (eb)	τ_{SF} (ps)	τ (ps)	Q_t (eb)
$15/2^-$	310	$71\ ^{+6}_{-5}$	$3.55^{+0.13}_{-0.15}$	1.1(2) ns	64.2(39)	3.74(1)
$19/2^-$	552	$3.9\ ^{+0.3}_{-0.2}$	$3.53^{+0.09}_{-0.13}$	1.9(2)	3.42(10)	3.77(6)
$23/2^-$	709	$1.43^{+0.1}_{-0.14}$	$3.09^{+0.16}_{-0.11}$	14(3)	–	–
$27/2^-$	813	<0.70	>3.18	–	–	–
$31/2^-$	864	<0.60	>2.89	–	–	–
$23/2^+$	682	$14.0^{+2.7}_{-3.3}$	–	–	–	–
$27/2^+$	488	<8	>3.3	–	–	–

shell correction were performed for the yrast band in ^{131}Ce using Woods–Saxon potential. In the TRS calculations three deformation parameters β_2, β_4 and γ, were used and the energy plots are minimized with respect to β_4. Figure 10 shows the results of TRS calculations at (a) low frequency ($\omega = 0.05$ MeV/$\hbar$) and (b), (c) at higher frequencies, $\omega = 0.25$ and 0.30 MeV/$\hbar$ respectively.

The calculations predict a near-prolate shape with deformation $\beta_2 = 0.21$ and $\beta_4 = -0.02$, at the beginning of the band. However, the shape is predicted to quickly become triaxial. This is seen from the TRS plots (figures 10b and 10c) at a rotational frequency of 0.25 MeV/$\hbar$ and 0.3 MeV/$\hbar$, where triaxiality is predicted to change from a value of $\gamma = -46°$ to $\gamma = -80°$, while β_2 value has changed just marginally from 0.21 to 0.23 (with $\beta_4 = 0.009$ and -0.003 respectively).

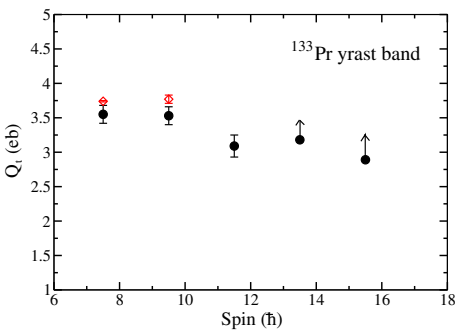

Figure 9. Transition quadrupole moment as a function of spin for the yrast band in ^{133}Pr. The points depicted by filled circles are from the present measurements while the points depicted by diamonds are determined from the lifetime measurements [31]

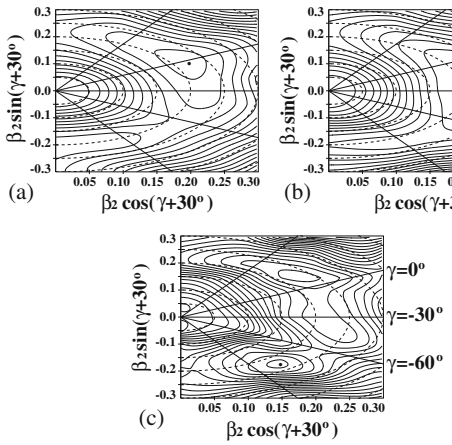

Figure 10. Total Routhian surfaces (TRS) for the yrast band based on $\nu h_{11/2}$, $(\pi, \alpha) = (-, -1/2)$ in ^{131}Ce. TRS plots at (**a**) frequency $\hbar\omega = 0.05$ MeV depicting a minimum close to a prolate shape with $\beta_2 = 0.21$ but softness in triaxility γ, (**b**) at frequency $\hbar\omega = 0.25$ MeV, depicting a minimum for a triaxial shape with $\beta_2 = 0.22$, $\gamma = -46°$ and (**c**) at frequency $\hbar\omega = 0.30$ MeV, depicting primary minimum at $\beta_2 = 0.23$, $\gamma = -80°$ and a secondary minimum at $\beta_2 = 0.22$, $\gamma = 10°$.

For a prolate shape, the deformation β_2 is related to the transition quadrupole moment (assuming no hexadecapole deformation) by

$$Q_t = \frac{3ZR^2}{\sqrt{5\pi}}\beta_2(1 + 0.36\beta_2), \quad (4)$$

where Z is atomic number of the nucleus and R is the radius of the nucleus given by $1.2A^{1/3}$ in fermi. If we take the average Q_t (see figure 5) as 3.2 eb (close to the beginning of the band), this leads to deformation $\beta_2 = 0.19$, which is in good agreement with the prediction of the TRS calculations ($\beta_2 = 0.21$) within the given experimental errors. For a non-axial shape, the measured transition quadrupole moment is related to the intrinsic quadrupole moment Q_{20} by the equation [36]

$$Q_t = Q_{20}\,\frac{\cos(\gamma + 30)}{\cos(30)}. \quad (5)$$

If we assume $\gamma = -80°$ as predicted by TRS calculations and use an average value of the measured $Q_t = 2.5$ eb for higher members of the band (refer to figure 5) then eq. (5) gives $Q_{20} = 3.37$ eb, which leads to $\beta_2 = 0.20$. This agrees quite well within the experimental errors, with the predicted value of $\beta_2 \sim 0.23$ from the calculations.

A typical plot of single quasiparticle level energy as a function of triaxiality parameter γ, for proton $\pi h_{11/2}$ and neutron $\nu h_{11/2}$ orbitals in this mass region as predicted by CHFB calculations is shown in figure 11. It is evident from this plot that, for a triaxiality value of $\gamma \leq -75°$, the unfavoured signature $\alpha = +1/2$ for $\nu h_{11/2}$ orbital is lower in energy and thus it can be said that at higher spins, $\alpha = +1/2$ is the signature for this band. Calculations by Granderath *et al* [4] had also predicted such a behaviour in this nucleus. This implies that at higher spins this band has a pair of aligned $h_{11/2}$ neutrons. This is consistent with the assignment of $\nu h^3_{11/2}$ by Palacz *et al* [11] for this band. Large signature splitting seen in this band [11] also supports high value of triaxiality in this band. In ^{133}Ce, a number of triaxial bands were reported by Hauschild *et al* [37], of which the most intensely populated band was assigned a $\nu(h_{11/2})^3$ configuration. Later, Joss *et al* [9] determined the value of triaxiality $\gamma = -83°$ and $\beta_2 \sim 0.19$ for this band, for spins above $19\hbar$. However, from the present study, it can be said that in the case of ^{131}Ce, similar triaxiality seems to develop even at a spin of about $16\hbar$ in the $\nu h^3_{11/2}$ band.

TRS calculations (figure 10c) also predicts a secondary minimum at $\beta_2 = 0.22$ and $\gamma = 10°$ at a frequency $\hbar\omega = 0.3$ MeV. This could arise when the proton orbitals $\pi h_{11/2}$ get active due to the alignment

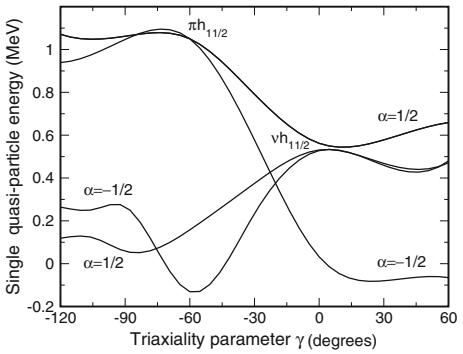

Figure 11. Single quasiparticle levels for proton $\pi h_{11/2}$ and neutron $\nu h_{11/2}$ orbitals in ^{131}Ce nucleus as a function of triaxiality parameter γ; the calculations were done at quadrupole deformation $\beta_2 = 0.2$ and rotational frequency of $\hbar\omega = 0.25$ MeV with pairing gap parameters for protons and neutrons Δ_p, Δ_n respectively, both equal to 1.2 MeV; the signature quantum number α, values are indicated on the orbitals.

of a pair of protons in $h_{11/2}$ orbitals leading to $\gamma = 0°$ or even to positive values of triaxiality (as predicted in figure 11 for $\pi h_{11/2}$ orbitals). Such a band was also observed in [11], close to this rotational frequency and this band becomes yrast at a spin of about $15\hbar$. In the present work, the γ lines from this band were seen but due to poor statistics no lifetimes could be measured for the states of this band. It is also worth noting that at higher frequencies it is seen from the TRS plots (figure 10c) that while the nucleus acquires significant triaxiality, the softness in this degree of freedom is significantly reduced.

6.2 ^{133}*Pr nucleus*

In figure 12, total Routhian surface (TRS) calculations for the yrast band based on the $\pi h_{11/2}$ orbital in ^{133}Pr are shown at the same rotational frequencies, $\omega = 0.05$, 0.25 and 0.3 MeV/$\hbar$, as in the case of ^{131}Ce nucleus. It is evident from the plots that TRS predicts a significant softness in the triaxiality degree of freedom in this nucleus. However, the minima for the frequencies shown, hovers around the prolate shape with an average deformation $\beta_2 = 0.22$. The values of triaxiality parameter predicted for these frequencies are insignificant; especially in the light of the fact that for TR surfaces flat in the triaxial degree of freedom, the numerical interpolations done to find the precise position of an energy minimum may not be exact. If we thus assume a prolate shape (as predicted for proton $\pi h_{11/2}$ orbitals in figure 11) for this nucleus, then near the band head, $Q_t \sim 3.6$ eb leads to a quadrupole

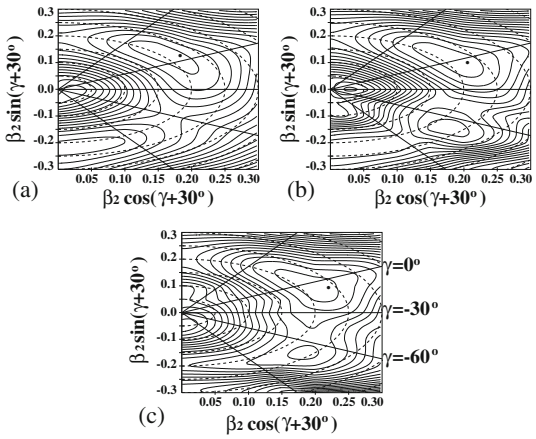

Figure 12. TRS plots for yrast band based on $\pi h_{11/2}$, $(\pi, \alpha) = (-,-1/2)$ in ^{133}Pr; (**a**) at $\hbar\omega = 0.05$ MeV minimum is predicted at $\beta_2 = 0.22$, $\gamma = 5°$, (**b**) at $\hbar\omega = 0.25$ MeV minimum is predicted at $\beta_2 = 0.22$, $\gamma = -2°$ and (**c**) at $\hbar\omega = 0.3$ MeV minimum is predicted at $\beta_2 = 0.23$, $\gamma = -5°$.

deformation $\beta_2 = 0.21$. This value is in good agreement with the predicted value ($\beta_2 = 0.22$) from TRS calculations for the quadrupole deformation.

The marginal reduction in the value of quadrupole moment Q_t (about 10%) in the experimental values at higher spins leads to a value of about 9° for the triaxiality parameter γ using eq. (3). Though this is less evident from the TRS plots due to the γ-softness of the TR surfaces, it can be seen from figure 11 that $\pi h_{11/2}$ tends to drive the nucleus towards small positive values of triaxiality. It can thus, be said that predictions of the cranked Hartree–Fock–Bogoliubov and TRS calculations that $\pi h_{11/2}$ orbital drives the nucleus towards a prolate shape with a deformation of $\beta_2 \sim 0.2$ is in agreement with the experimental observations. The neighbouring nucleus ^{131}La also has yrast band based on a decoupled odd proton in low $\Omega h_{11/2}$ orbital. Zamfir *et al* [38] have measured lifetimes of the states in the yrast band and the values of transition quadrupole moment (based on these measurements) stay around 3.24 eb up to a spin of $23/2\ \hbar$ and then drop to about 2.9 eb. This behaviour is consistent with the behaviour in ^{133}Pr found in context of the shape polarization property of low $\Omega h_{11/2}$ orbital. Grodner *et al* [30] have measured the lifetimes for levels with spin $I \geq 23/2\ \hbar$ in the yrast band in ^{131}La and their measurements are in agreement with ref. [38].

It is important to note that these predictions (and observations) are before the band-crossing frequency which is beyond 0.4 MeV/$\hbar$ [12] in this band and hence more straightforward to make conclusions about the shape driving property of the $\pi h_{11/2}$ orbital which otherwise becomes difficult due to the mixing of different orbitals.

7. Summary

In summary, lifetime measurements of states in the yrast band in ^{131}Ce based on a decoupled neutron $\nu h_{11/2}$ orbital and in ^{133}Pr based on a decoupled proton $\pi h_{11/2}$ orbital were done using the plunger method and the Doppler-shifted attenuation method. In ^{131}Ce, lifetimes of four states were determined and limits were found for three states. In ^{133}Pr, lifetimes were determined for four states (of which one state belongs to a positive-parity non-yrast band) and upper limits for three states were found. From the experimentally determined values of lifetimes, transition quadrupole moments and the deformation parameters β_2 and γ were extracted.

The results of TRS calculations based on the cranked Hartree–Fock–Bogoliubov (CHFB) with Strutinsky's shell correction approach agree quite well with the extracted values of the shape parameters. In the case of ^{131}Ce, the neutron, $\nu h_{11/2}$, high Ω orbital seems to drive the shape of the nucleus to high triaxiality of about $\gamma = -80°$ at higher spins in the yrast band, while the low Ω proton, $\pi h_{11/2}$ orbital in ^{133}Pr seems to stabilize the shape of the nucleus to almost zero triaxiality, i.e., prolate shape. In both cases, the quadrupole deformation β_2 stays close to 0.22. These observations are in conformity with the γ shape driving properties of low and high $\Omega h_{11/2}$ orbitals in these γ-soft nuclei as envisaged in the framework of the CHFB model.

Acknowledgements

The authors extend their thanks to the Pelletron crew of Inter University Accelerator Centre, New Delhi for providing excellent beams during the experiments and the target laboratory for their help in preparing the targets. The authors would also like to thank Prof. J C Wells for providing the lifetime analysis programs LIFETIME and LINESHAPE. The authors are grateful to Dr A Roy for his guidance and support throughout this work.

References

[1] H A Jahn and E Teller, *Proc. R. Soc. London A* **161**, 220 (1937)
[2] J Dudek *et al*, *Phys. Rev. Lett.* **97**, 072501 (2006)
[3] M Yamagami *et al*, *Nucl. Phys. A* **693**, 579 (2001)
[4] A Granderath *et al*, *Nucl. Phys. A* **597**, 427 (1996)

[5] R W Laird *et al*, *Phys. Rev. Lett.* **88**, 152501 (2002)
[6] Y S Chen *et al*, *Phys. Rev. C* **28**, 2437 (1983)
[7] E S Paul *et al*, *Phys. Rev. Lett.* **58**, 984 (1987)
[8] G Andersson *et al*, *Nucl. Phys. A* **268**, 205 (1976)
[9] D T Joss *et al*, *Phys. Rev. C* **58**, 3219 (1998)
[10] E S Paul *et al*, *Nucl. Phys. A* **690**, 341 (2001)
[11] M Palacz *et al*, *Z. Phys. A* **338**, 467 (1991)
[12] L Hildingsson *et al*, *Phys. Rev. C* **37**, 985 (1988)
[13] W Nazarewicz *et al*, *Nucl. Phys. A* **435**, 397 (1985)
[14] T Bengtsson *et al*, *Nucl. Phys. A* **436**, 14 (1985)
[15] R Wyss *et al*, *Phys. Lett. B* **215**, 211 (1988)
[16] G K Mehta *et al*, *Nucl. Instrum. Methods A* **268**, 334 (1988)
[17] P Joshi, *A study of shape deformation at high spins in deformed nuclei,* Ph.D. Thesis (Punjab University, 2000) p. 91
[18] P Joshi *et al*, *Phys. Rev. C* **60**, 034311 (1999)
[19] T K Alexander *et al*, *Nucl. Instrum. Methods* **81**, 22 (1970)
[20] R P Singh *et al*, *Eur. Phys. A* **7**, 35 (2000)
[21] Yu Khazov *et al*, *Nuclear Data Sheets* **107**, 2715 (2006)
[22] A Dewald *et al*, *Z. Phys. A* **334**, 163 (1989)
[23] J C Wells *et al*, Report No. ORNL/TM-9105 (1985)
[24] J Srebrny *et al*, *Nucl. Phys. A* **683**, 21 (2001)
[25] F James *et al*, *Comput. Phys. Commun.* **10**, 343 (1975)
[26] J C Wells *et al*, *LINESHAPE: A computer program for Doppler-broadened lineshape analysis,* Report No. ORNL-6689, 1991
[27] J F Ziegler, *The stopping and ranges of ions in matter* (Pergamon, London, 1985) Vols 3 and 5
[28] L C Northcliffe *et al*, *Nucl. Data Tables* **7**, 233 (1970)
[29] J Gizon *et al*, *Nucl. Phys. A* **290**, 272 (1977)
[30] E Grodner *et al*, *Eur. Phys. A* **27**, 325 (2006)
[31] T Klemme *et al*, *Phys. Rev. C* **60**, 034301 (1999)
[32] G-S Li *et al*, *Chin. Phys. Lett.* **21**, 461 (2004)
[33] M P Fewell *et al*, *Phys. Rev. C* **37**, 101 (1988)
[34] F S Stephens, *Rev. Mod. Phys.* **47**, 43 (1975)
[35] Yu Khazov *et al*, *Nuclear Data Sheets* **112**, 855 (2011)
[36] A V Afanasjev *et al*, *Nucl. Phys. A* **591**, 387 (1995)
[37] K Hauschild *et al*, *Phys. Rev. C* **54**, 613 (1996)
[38] N V Zamfir *et al*, *Z. Phys. A* **344**, 21 (1992)